BMC Biology

RESEARCH ARTICLE

Open Access

Bio-informed synthesis of marine-sourced indole derivatives: suppressing gram-negative bacteria biofilm and virulence

Karina Golberg[1†], Kamal Elouarzaki[2†], Bat-el Kagan[1], Marilou Shagan[1,3], Netta Shemesh[4], Esti Kramarsky-Winter[1], Anat Ben-Zvi[4], Yaffa Mizrachi Nebenzahl[3,5^], Robert S. Marks[1,6] and Ariel Kushmaro[1,6,7*]

Abstract

Biofilms cling to surfaces to form complex architectures allowing their bacterial creators to acquire multidrug resistance and claiming countless lives worldwide. Therefore, finding novel compounds that affect virulence and biofilm-forming capacity of resistant pathogenic bacteria is imperative. Recently, we identified indole-based compounds that possess anti-biofilm properties in coral-associated bacteria. We succeeded in efficiently synthesizing two of these compounds, 1,1′-bisindole (NN) and 2,3-dihydro-2,2′-bisindole (DIV). They were found to attenuate biofilms of gram-negative bacterial pathogens, including *Pseudomonas aeruginosa* and *Acinetobacter baumannii*. Combining these compounds with the antibiotic tobramycin resulted in significant biofilm inhibition, particularly in the eradication of mature *P. aeruginosa* biofilms. Both of the bisindole derivatives, suppressed a number of bacterial virulence factors, reduced bacterial adhesion, and improved survival rates in infected *Caenorhabditis elegans* and human lung epithelial cell models. Transcriptome analyses of the bacteria treated with these compounds revealed that NN repressed or upregulated 307 genes when compared to untreated *P. aeruginosa*. These bacteria-derived molecules act in resistance-quenching and are potentially important candidates for inclusion in treatment protocols. The use of compounds that prevent the biofilm from accumulating the high cell densities critical to its structural and functional maintenance represents significant progress in the management of bacterial persistence. Therefore, a possible clinical implementation of these innovative compounds holds a promising future.

Keywords Antibiotics, Biofilm eradication, Bis-indoles, Chemical biology, Resistance

†Karina Golberg and Kamal Elouarzaki contributed equally to this work.

^Yaffa Mizrachi Nebenzahl is deceased.

*Correspondence:
Ariel Kushmaro
arielkus@bgu.ac.il
[1] Department of Biotechnology Engineering, Avram and Stella Goldstein-Goren, Ben-Gurion University of the Negev, Beer-Sheva 84105, Israel
[2] School of Materials Science and Engineering and Center for Advanced Catalysis Science and Technology, Nanyang Technological University, 50 Nanyang Avenue, Singapore 639798, Singapore
[3] Pediatric Infectious Disease Unit, Faculty of Health Science, Soroka University Medical Center, Beer-Sheva 84105, Israel
[4] Department of Life Sciences, Ben-Gurion University of the Negev, Beer-Sheva 84105, Israel
[5] Department of Microbiology and Immunology, Faculty of Health Sciences, Ben-Gurion University of the Negev, Beer-Sheva 84105, Israel
[6] The Ilse Katz Center for Nanoscale Science and Technology, Ben-Gurion University of the Negev, Beer-Sheva 84105, Israel
[7] School of Sustainability and Climate Change, Ben-Gurion University of the Negev, Beer-Sheva 84105, Israel

Background

The emergence of broad-spectrum antibiotic-tolerant pathogens remains a leading cause of death that claims millions of lives every year worldwide [1–3]. Many severe chronic and acute resistant infections are the result of the establishment of opportunistic pathogens on surfaces that are in intimate contact with animal tissues. To establish infection in vivo, the bacteria exploit two pathways of invasion: a massive toxin secretion as part of the acute attack, and surface-anchoring settlement, which bacteria exploit to establish a persistent biofilm [4, 5]. The ability of these pathogens to secrete an extracellular matrix that enables bacteria to establish footholds that manifest as biofilms on a variety of surfaces is a prominent feature of chronic infections [6].

Effectively a bacterial mat, the biofilm is characterized by a complex, three-dimensional arrangement that provides a structural framework and a reservoir for self-protected bacterial cells, shielding them from intensive antibiotic treatments or from innate and adaptive host defenses [6–8]. These protective mechanisms, in turn, complicate the eradication of pathogens, which are especially deleterious when the host defense mechanism is compromised. This is because these bacterial protective mechanisms result in the constant exhaustion of the host defense system, persistent inflammation, and extensive tissue damage [9, 10]. Accumulating evidence from studies of the biofilms with such protective mechanisms indicates that some gram-negative pathogenic bacterial strains produce biofilms with global antibiotic resistance [11, 12]. According to World Health Organization (WHO) global priority list of gram-negative-resistant pathogens, two species, *A. baumannii* and *P. aeruginosa* are categorized as critical threat [12].

The ability of these pathogenic bacteria to grow in biofilm-forming communities stems from a behavioral characteristic known as "bacterial socialization" that is governed by the widely conserved quorum sensing (QS) regulatory mechanism [13, 14]. The synchronized social behavior mediated by QS effectively regulates specific gene sets that control the production of signal molecules and receptors that together constitute an important part of the entire set of bacterial communication processes [15]. The language messages activate the transcription of specific target genes, including those involved in biofilm formation and virulence behavior. Together with an arsenal of cell-associated and extracellular virulence factors, they mediate infection pathogenesis [16, 17].

The grave threat posed to human health by the growth in bacterial resistance to conventional antibiotic regimens dictates the need to develop alternative treatment strategies. To mitigate infection pathogenesis, interference with biofilm integrity and with virulence, constitute a promising strategy to combat antibiotic-resistant infections. The search for novel anti-biofilm candidates led us to the marine environment, where many natural products with anti-biofilm activity have been identified [18]. The coral-associated bacterial community is highly complex. It is known to produce a wide variety of metabolites that effectively prevent pathogenic species from initiating a disease process without unleashing any toxic effects on their animal partners [19, 20]. In a study by Golberg et al. (2013), coral-associated bacteria were isolated and tested for their anti-QS and anti-biofilm activities [21].

In our current study, we successfully identified and analyzed the structures of two potent compounds—1,1'-bisindole (NN) and 2,3-dihydro-2,2'-bisindole (DIV). These compounds hold immense biological potential, but their natural sources are scarce. Additionally, their chemical composition is complex, making it a challenge to obtain them in pure form. Therefore, we employed a highly efficient and practical chemical synthesis method to produce ultrapure quantities of NN and DIV. We then investigated the effects of these synthesized compounds and their impact on the biofilm of the most prioritized threatening bacterial pathogens, virulence, adhesion, gene expression, sensitivity to antibiotics, and their possible modes of action on model bacterial pathogens.

Results and discussion

In the post-antibiotic era, the quest for novel bioactive compounds has focused on biofilm attenuators and other compounds that selectively block virulence traits [22–24]. This strategy, motivated by the understanding that resistant chronic infections may occur in the form of persistent biofilms, has led to the search for a variety of sources for novel products that attenuate biofilm development. Indeed, a rigorous investigation of commercially important metabolites and their associated producers revealed that bacteria themselves may represent a considerably productive source of such metabolites [25–27]. The understanding that resistant chronic infections may occur in the form of persistent biofilms in tissues or on organismal surfaces has led to the search for novel treatments to combat these persistent infections. In this study we utilized an emerging source for bioactive microorganisms, the coral reef ecosystem which is a veritable gold mine of natural resources for diverse, new, potentially applicable bioactive metabolites. Indeed, in our previous study, we used bioreporter bacterial strains to show that 40% of the coral mucus-associated bacteria not only exhibited QS inhibition activities [21, 28], they also possessed anti-biofilm properties. We therefore harnessed this knowledge to investigate and demonstrate two active compounds derived from coral associated

microorganisms, *1,1'-bisindole (NN) and* 2,3-dihydro-2, 2'-bisindole *(DIV)* with possible anti-biofilm properties.

Chemical identification of the two active compounds 1,1′-bisindole (NN) and 2,3-dihydro-2, 2′-bisindole (DIV)

The coral-associated bacteria's active compounds, NN and DIV, underwent isolation and identification through UV, LC/MS, MS, and NMR techniques.

1,1′-bisindole (NN)

The ion peak measurement for NN using mass spectrometry showed an observed mass of 233.1000, which corresponds to the molecular formula C16H12 N2 with 12 hydrogen deficiency indices. The required m/z for [M + H] is 233.0078. The UV absorption maxima observed at 218 nm indicated an indole moiety. In the ^{1}H NMR spectrum of NN, signals between 6.5 and 7.8 were typical of an indole skeleton and could be assigned to aromatic and hetero-aromatic rings. The ^{13}C NMR spectrum also showed all signals required for an indole skeleton. These signals confirmed the presence of a partial indole skeleton structure. Based on the molecular formula and mass, it was evident that only one of the two identical parts of the molecule displayed the ^{1}H and ^{13}C NMR signals. This indicated that the molecule contained two similar parts. To explain the formula and molecular mass of the molecule, we proposed three hypotheses by combining two indole structures, with the only difference being the position and nature of the bridge (N–N or C–C) connecting the two indole units. However, due to the impure state of the natural compound NN, it was challenging to confirm any of our hypotheses. Therefore, we opted to synthesize the N–N bridge structure and subjected it to MS and NMR analysis to determine the final structure conclusively by direct comparison to the natural fraction NN.

Figure 1 displays the process of synthesizing NN, which involves a simple and straightforward procedure that begins with using indole as the starting compound. The reaction takes place in the presence of a rare earth metal amide $[(Me_3Si)_2N]_3Y(\mu\text{-}Cl)Li(THF)_3$. The reaction initiates with the creation of a rare earth metal amido complex, which, when exposed to air, releases an N-radical. This N-radical then undergoes dimerization, resulting in the formation of the corresponding symmetrical N–N coupled indole product.

The ^{1}H NMR spectrum ($CDCl_3$) of the final product was simple and had only six signals. These included two doublets at 6.67 and 6.89, two triplets at 7.16 and 7.20, a doublet at 7.32, and a double doublet at 7.22 and 7.14. Each of these signals integrated for one proton. On the other hand, the ^{13}C NMR spectrum showed only six signals from aromatic methines and two quaternary carbons. These results confirmed that the indole dimer is symmetric and connected through an N–N bridge. An additional 2D NMR HSQC experiment verified the presence of a system of consecutive methines in each heteroaromatic and aromatic ring, confirming the existence of an indole nucleus without additional quaternary carbon. Based on these findings, the natural fraction NN and the synthesized product had similar characteristics, and the fraction was confirmed to contain 1,1'-bisindole (NN).

2,3-dihydro-2, 2′-bisindole (DIV)

The DIV isolated fraction was found to be a bisindole derivative with a $[M + H]^+$ of 235 and 11 hydrogen deficiency indices. The presence of an indole moiety was suggested by UV absorptions at 214 and 258 nm. The ^{1}H NMR signals of DIV showed two double doublets between δ 3.0 and 4.0, each integrated for 1 proton with a total proton number of 14. This indicated an asymmetric structure with one methylene located in the heteroaromatic ring. The ^{13}C NMR and 2D experiments confirmed the structure and assignments, with an HSQC experiment establishing the existence of a system of four consecutive methines for each aromatic ring. Furthermore, the heteronuclear multiple bond correlation experiment showed correlations between the protons and the quaternary carbons, confirming an indole nucleus with a quaternary carbon at position 2 (C–C bridge). Additional spectral data allowed for the identification of DIV as 2,3-dihydro-2,2'-bisindole, which was confirmed through chemical synthesis. The chemical shifts were in good agreement with the natural product.

A variety of indole compounds possessing a wide range of biological/pharmacological properties, including anti-biofilm activities, have been isolated from the marine environment [29]. Certain gram-positive and gram-negative bacteria, including pathogenic species, were shown to produce indole via the tryptophan biosynthetic pathway [30, 31]. Furthermore, even those that do not directly synthesize indoles are able to produce indole derivatives through enzymatic modifications [19]. One such example includes members of the mammalian gut microflora that have been implicated in the metabolic conversion of indole to the potent antioxidant indole-3-propionic acid (IPA) [19]. Additionally, antimicrobial properties have been found in many natural indoles, such as vibrindole A and turbomycin A, which are produced by the marine bacteria *Vibrio parahaemolyticus* [32, 33]. Indole-based derivatives also seem to play an important role in inter-kingdom signaling [34], and although they are not produced by the eukaryotes themselves, they are known to affect host health [19]. Therefore, the biological activities of the bisindole compounds discovered in the present study were investigated in terms of their ability

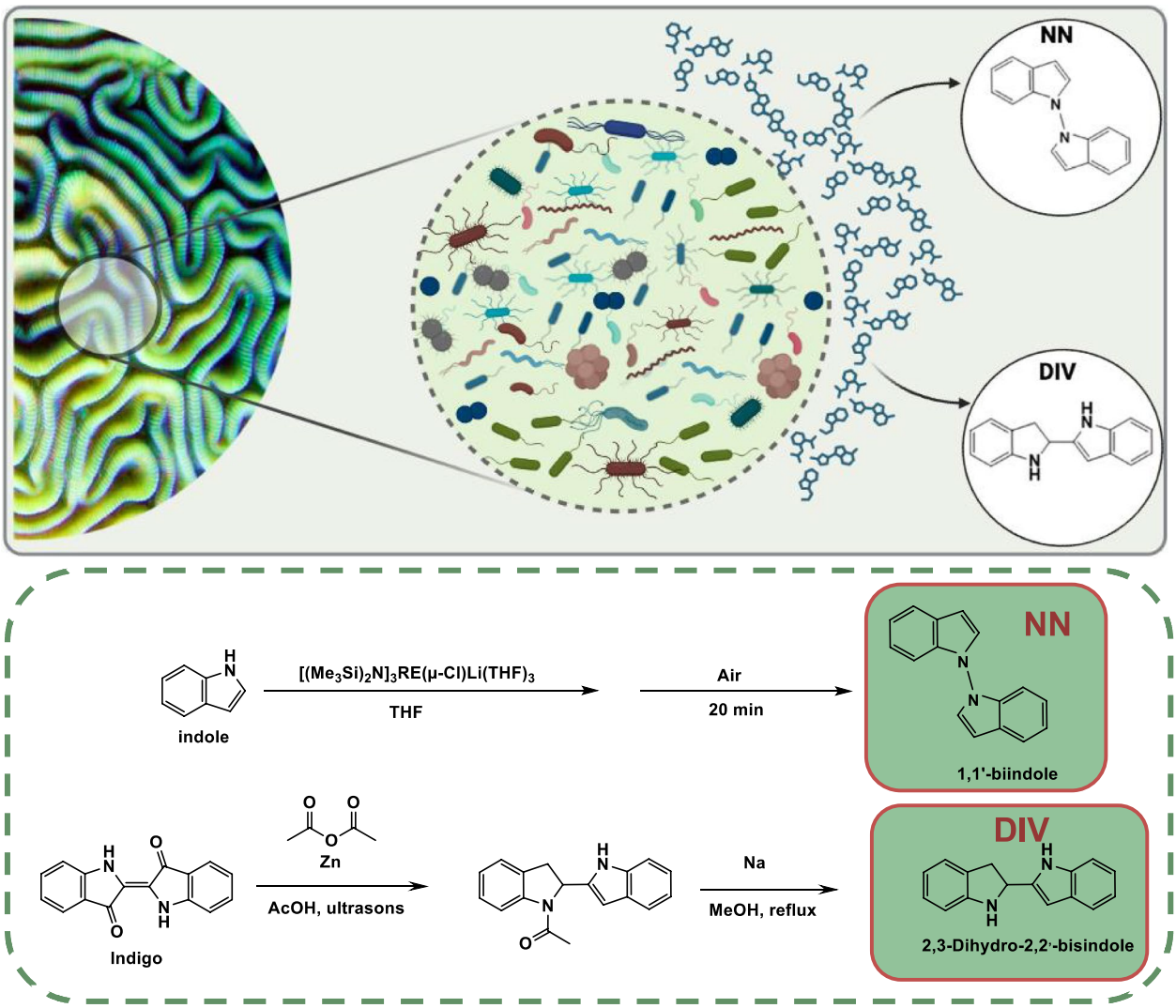

Fig. 1 Active compounds isolations from coral-associated bacteria and synthetic pathways of the indole-based compounds

to attenuate the biofilm related activities and impact on virulence.

The effect of indoles on biofilm formation by model bacteria

The importance of mitigating biofilm initiation and maintenance in the medical and industrial settings stems from the understanding that resistant chronic infections may occur in the form of persistent biofilms in tissues or on organismal surfaces. The premise is that pathogenicity of biofilm can be reduced by exploiting compounds that inhibit the regulation pathway required to establish and maintain a resistant biofilm. To verify this, an assay to examine this ability was developed using a number of relevant pathogenic bacteria strains including *P. aeruginosa*, *A. baumannii*, *Serratia marcescens*, and *Providencia stuartii.* We then tested the effectiveness of the bisindole compounds on the biofilm forming bacteria. Since inadequate amounts of indole containing compounds were obtained from the coral associated bacterial cultures themselves, it was necessary to use equivalent synthetic products. The model bacterial biofilm strains were allowed to develop on glass slides and their densities and viabilities of the bacterial biofilms were assayed using live/dead stains, SYTO 9 (stains live cells green) and propidium (PI) iodide (stains dead cells red). This method enabled the live and dead cells to be visualized using confocal scanning laser microscopy (CSLM) (Fig. 2, Additional file 1: Fig. 1S). Since biofilm density and viability depend on a number of parameters, including attachment, growth, and mortality of the bacterial strains, we evaluated each of these parameters separately and in combination.

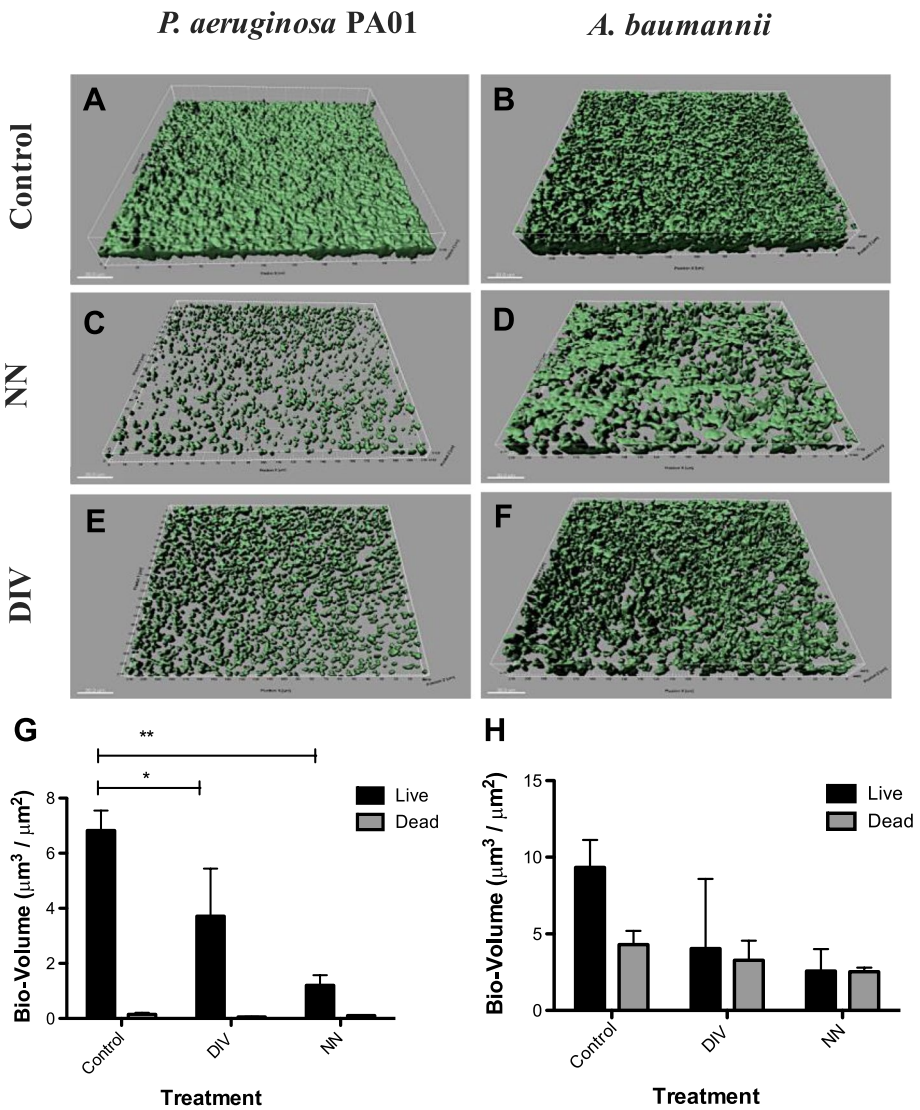

Fig. 2 Prevention of biofilm formation. Confocal laser scanning micrographs of *P. aeruginosa* PA01 (**A**, **C**, **E**) and *A. baumannii* (**B**, **D**, **F**) formed in glass-bottomed 96-well plates after 18 h of static incubation at 37 °C. Cultures were grown in the presence of 50 μM of either DIV or NN or an equivalent amount of DMSO for control. Biofilms were stained using the Live/Dead bacterial viability kit. Only the live cells are represented since the dead fraction was not significant between the groups. Live, dead, and total bio-volumes ($\mu m^3/\mu m^2$) were calculated based on image analysis and data from the IMARIS software for (**G**) *P. aeruginosa* PA01 and (**H**) *A. baumannii*. Bars indicate standard deviations for triplicate sets of experiments. Differences were analyzed for their significance by using one-way ANOVA with Tukey's test. ** $P < 0.001$ and * $P < 0.01$

A comparison of biofilm density following treatment with 50 μM 1,1'-bisindole (NN) or 2,3-dihydro-2,2'-bisindole (DIV) (Fig. 2A–F) showed that although both treatments led to reductions in the density of attached cells, the extent of the reduction varied depending on the treatment and on the bacterial strain. *P. aeruginosa* was inhibited by 45% by DIV and by 82% by NN, while *A. baumannii* was inhibited by 56% by DIV and by 72% by NN. Overall, NN was more effective at reducing *P. aeruginosa* density (Fig. 2G, H), while both the NN and DIV treatments had smaller effects on the density of *A. baumannii*. Both treatments caused only negligible bacterial cell mortality in *P. aeruginosa* and had no effect on the numbers of dead cells in the *A. baumannii* biofilm, which did not differ from the control.

When observing the chemical structures in the context of activity, the amine group in NN is not available for molecular interaction as it is used as the linker between two rings. On the other hand, the amine group in DIV is available for molecular interaction with corresponding cellular receptors, but it is found at different distances from the linker between the two rings. It therefore can

be assumed that this amine group may be the active site of this compound as indicated by both the differences in biofilm inhibition percent together with the compound structures. Liu et al. (2010) screened different molecules as QSI of *Pseudomonas aeruginosa* and also demonstrated that the amine moiety plays an important role in the inhibitory activity [35].

The high cell densities typical of mature biofilms provide the biofilm producers with a first line of defense by preventing competitors from penetrating the biofilm. The alterations in the structures or the reduction in the densities of attached cells that result from the application of these indole derivatives, enables other antimicrobials to penetrate developed biofilms, since biofilm establishment in long-term, chronic infections is enabled primarily by bacterial persistence [36].

Based on this logic, we challenged a mature *P. aeruginosa* biofilm with 50 μM NN compound to investigate whether NN-mediated biofilm disruption increased the antibiotic sensitivity of the bacterial biofilm (Fig. 3A–D). NN was selected for this analysis based on its stronger activity relative to that of DIV in the static assay setup (Fig. 2). Antimicrobial susceptibility patterns of various antimicrobial agents were determined prior to the addition of 20 μg/ml tobramycin by assessing MICs (Additional file 1: Table 1S). For tobramycin, an antibiotic commonly prescribed to CF patients with *P. aeruginosa* infections [37], the lowest MIC value was observed for NN, with a 44% increase in susceptibility. Treatment of the biofilm with NN alone reduced the biofilm by 81%, but it did not completely eradicate it (Fig. 3B, E). On the other hand, when the biofilm was treated with both tobramycin and NN, despite an increase in its bio-volume, half of the biofilm was eradicated, and the bacterial cells died (Fig. 3D, E). The observation of larger bio-volumes following the combined treatment was previously reported by our group [38], but this phenomenon is still not fully understood. A possible explanation may be that by inducing a stress response, the bacterial community compensates by accelerating the biofilm formation process, which results in a thicker biofilm. NN, however, was able to restore the efficacy of tobramycin without affecting the biofilm dispersal stage. Treatment of previously differentiated biofilms with a combination of NN and tobramycin resulted in the extensive death of biofilm forming cells. This combination promoted the eradication of a large part of the biofilm by facilitating deeper penetration of the biofilm by the antibiotics. Moreover, while treatment with 50 μM NN alone resulted in a thinner and more dispersed biofilm, it did not affect the viability of its components (Fig. 3B). Conversely, treatment with 20 μg/ml tobramycin alone increased the bio-volume, but neither the structure nor the viability of the biofilm was significantly affected (Fig. 3C).

Indeed, similar studies showed that when combined with tobramycin, baicalin hydrate, a known virulence and biofilm inhibitor, increased the survival of bacteria-infected *C. elegans* and accelerated the clearance of *Burkholderia cenocepacia* from the lungs of mice by increasing bacterial biofilm susceptibility to the antibiotic

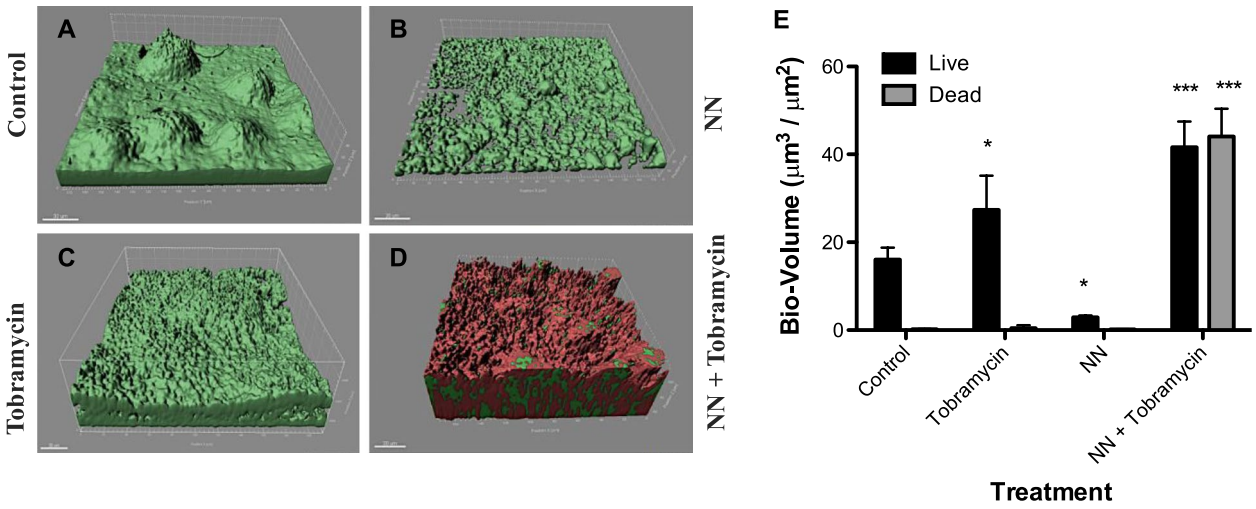

Fig. 3 Destruction of *P. aeruginosa* PA01 mature biofilm and sensitivity to antibiotics. CLSM of biofilm formed in a flow cell after 120 h of incubation at 37 °C (**A**), after 72 h of incubation alone and then 48 h of incubation in the presence of 50 μM NN (**B**), 20 μg/ml Tobramycin (**C**), or 50 μM NN with 20 μg/ml tobramycin (**D**). Biofilms were stained with the Live/Dead bacterial viability kit. Quantification of bio-volume (**E**): live, dead, and total bio-volumes ($\mu m^3/\mu m^2$) were calculated based on image analysis and data from IMARIS software. For each treatment, the images were acquired from three different areas. Results that were significantly different from the control based on a one-way ANOVA with Tukey's test are labeled with *** $P < 0.0001$ and * $P < 0.01$

[39, 40]. Therefore, combination treatments of antibiotics with anti-virulence compounds can complement host immunity defense [41, 42]. Such composite treatments support the results of earlier studies that indicated that *Vibrio*-derived polysaccharides increased the ability of aminoglycoside antibiotics to eradicate *P. aeruginosa* biofilm [43]. By harnessing our knowledge of the dynamic growth conditions in flow cell systems as models of the conditions in humeral tissues where pathogens thrive in enriched settings, we demonstrated that our inhibitor compounds can not only prevent biofilm development, they can also destroy already structurally developed biofilms of *P. aeruginosa* PA01. Developing such a treatment is of great importance with regard to mitigating biofilm initiation and maintenance in medical and industrial settings.

Assessment of virulence

As part of the arms race between pathogens and hosts, persistent intracellular pathogens have developed strategies for evading evolutionarily conserved defense mechanisms, thereby enabling them to establish infection in their hosts without causing death to the latter [44]. One such bacterial strategy manifests in the attenuation of bacterial virulence itself, a process that affects bacterial internalization and reduces host cell apoptosis. The treatment of *P. aeruginosa* with DIV or NN (50 µM) affected bacterial virulence by depressing the expressions of several *P. aeruginosa* virulence factors (Fig. 4A), chief among which were pyocyanin, elastase, and pyoverdine. The same three factors were also highly inhibited by NN, which also exhibited good inhibition of proteinase. Inhibition by DIV was greatest against the enzyme elastase (50%), while pyocyanin was the compound most strongly inhibited by NN (40%). Chitinase and pyocyanin were both strongly inhibited by both DIV and NN (Fig. 4A). The positive control, on the other hand, showed an inhibition of lipase of approximately 70% (Fig. 4A).

Bacteria rely critically on virulence factors to drive their pathogenicity. One such factor, Elastase, a proteolytic enzyme that destroys host elastin fibers and enables bacteria to invade tissues, was significantly reduced by both compounds [45]. Marked attenuation of pyocyanin by either DIV or NN, which is known to affect host cell respiration, ciliary function, and calcium homeostasis [46]. NN and DIV also showed strong inhibition of pyoverdine, an enzyme that plays a role in iron acquisition in *P. aeruginosa* that also influences its pathogenesis and virulence [47]. In addition to testing these compounds on bacteria, we evaluated their effects on bacterial infections in higher organisms by using the nematode *C. elegans* and the *A549* human lung cell line infected by *P. aeruginosa*.

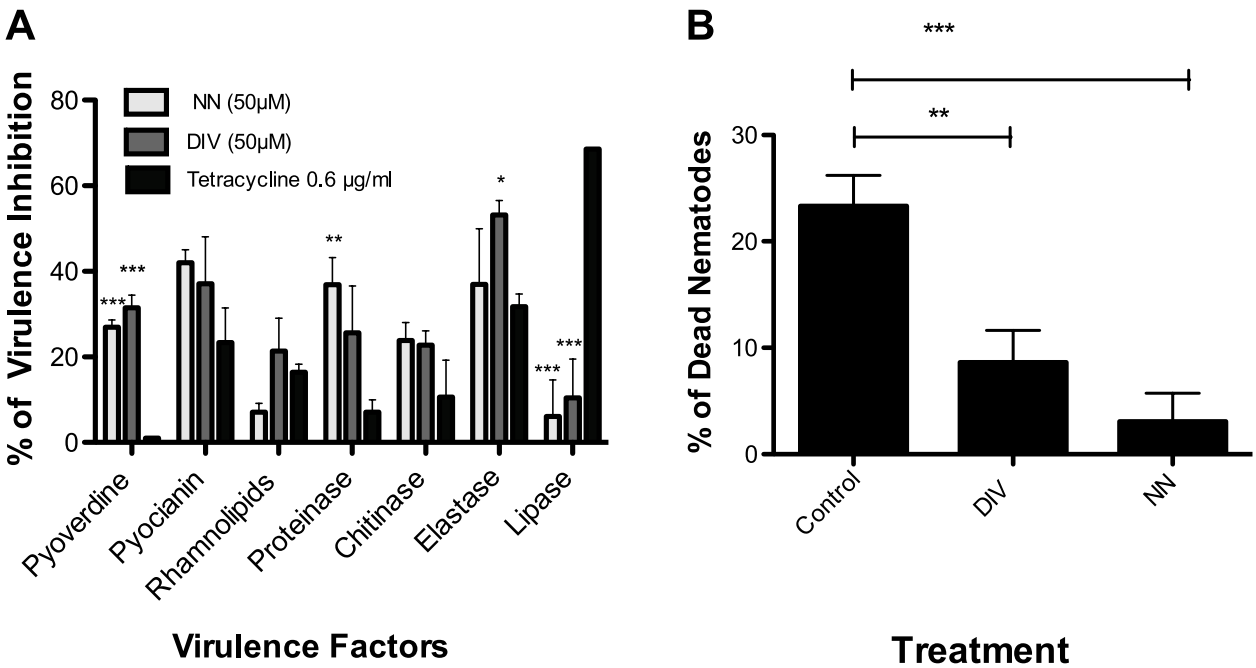

Fig. 4 Inhibition of virulence factor production in *P. aeruginosa* PA01 grown in the presence of 50 µM NN or DIV (**A**). Tetracycline treatment was used as positive control. Results are percent of inhibition distinctive to each factor and normalized to bacterial growth at OD600 nm. Error bars represent SD of three independent repetitions. Asterisks indicate significant differences when compared to tetracycline. *C. elegans* killing assay by *P. aeruginosa* PA01 assessed by SYTOX Orange stain over 24 h (**B**). Significance was determined by using one-way ANOVA with Tukey's test. *** $P < 0.0001$, ** $P < 0.001$, and * $P < 0.01$

Treatment with our compounds demonstrated prolonged survivorship in the nematode *C. elegans* (Fig. 4B), a model for host pathogen interaction in higher, multicellular organisms [48]. This finding indicates that the two treatments may have activated the nematode immune system. Exposure of *C. elegans* to a broad range of pathogens including *P. aeruginosa* may lead to the induction of resistance genes [35, 49]. Measuring nematode survival following exposure to *P. aeruginosa* in the absence and presence of modulating compounds provides a good model for assessing the effectiveness of the bisindole compounds on bacteria pathogenesis and on animal cell survival. The improved survival of *C. elegans* following its exposure to the pathogen in combination with either of our compounds showed that *P. aeruginosa* pathogenesis was reduced. Host mortality was reduced by 85 and 64% following pathogen exposure to NN and to DIV, respectively, compared to nematodes exposed to the pathogen alone. Thus, NN increased nematode survival significantly, resulting in the near complete rescue of the viability of the animals (Fig. 4B).

Pathogenesis attenuation was also tested using cultured human A549 lung cells. In the tissues of higher organisms, pathogen attenuation may occur through normal processes of bacterial clearance via the activation of innate and adaptive immune responses [50]. Bacterial clearance may be achieved either by physical sloughing of the bacteria or via their internalization by epithelial cells in a process that may then be followed by host cell apoptosis and subsequent phagocytosis of the infected cell [44].

Such processes can explain why bacterial persistence is usually impeded in healthy tissues but not in stressed tissues. The findings indicate that the apoptosis stage was delayed (Fig. 5A) when *P. aeruginosa* was exposed to the 50-μM dosage of either the NN or the DIV compound. This observation is in the line with a decreased ability of *P. aeruginosa* to adhere to epithelial cells (Fig. 5B), which probably also explains the pathogen's reduced cytotoxic effect.

The release of adherent bacteria from cell surfaces can be monitored as an indication of its ability to infect. Our results showed that culturing the pathogenic *P. aeruginosa* in either of the compounds (NN or DIV) caused their release from the cell surfaces in similar percentages that differed significantly from that of the untreated control (Fig. 5B). This observation supported the effectiveness of both treatments in attenuating pathogen ability to adhere to the model cells.

Mode of regulation

To elucidate the regulation of these compounds, we generated expression maps of the genes of our model biofilm forming bacterium *P. aeruginosa* after its exposure to either NN or DIV and compared them to the gene expression map of the control using transcriptional analysis. Results of gene expression mapping revealed totals of 7 and 304 genes in *P. aeruginosa* that were differentially expressed following exposure to DIV and NN, respectively, compared to the control (Fig. 6A, Additional file 1: Figs. 2S- 3S). These genes were then submitted to hierarchical clustering, and subsequent exposure of *P.*

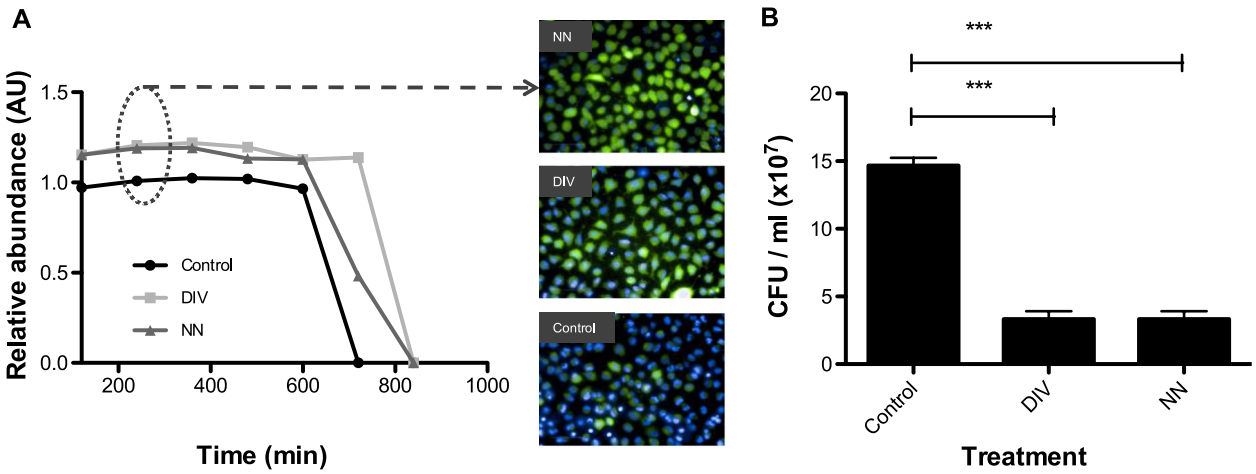

Fig. 5 Cytotoxicity effect and apoptosis of A549 cells pre-treated with *P. aeruginosa* PA01 over 14 h. A549 cells were infected with *P. aeruginosa* at a MOI of 40. Infection progress was monitored by measuring calcein staining intensity using the Operetta screening system; the signals were normalized to those obtained from equivalent reactions without bacterial component (**A**). All experiments were performed in triplicate. The effect reflected reduced adhesion of *P. aeruginosa* PA01 in the human A549 lung cell model (**B**). Adhesion of pre-treated *P. aeruginosa* PA01 (10^7 CFU/ml) to A549 cells following 1 h of incubation. Excess bacteria were removed, and the released cells were plated to determine CFU counts. Differences were analyzed for their significance by using one-way ANOVA with Tukey's test. ***, $P < 0.0001$

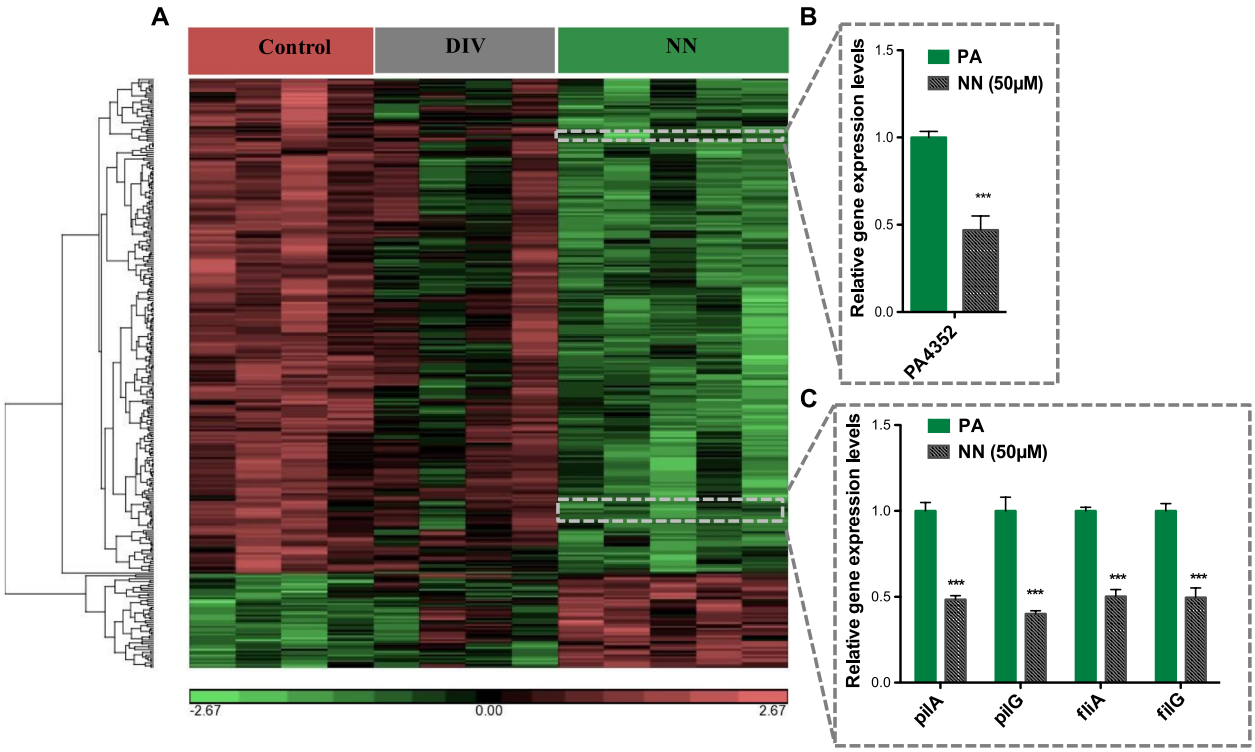

Fig. 6 Gene-wise hierarchical clustering of the 307 genes found to be differentially expressed in each treatment compared with the control (DIV vs. DMSO, NN vs. DMSO). Prior to clustering, expression signals were standardized so that the mean of each gene was 0 and the standard deviation was 1. Pearson's dissimilarity and complete linkage were used for the clustering. A gene was defined as differentially expressed in a certain contrast if it fulfilled all of the following criteria: nominal *p*-value < 0.01; linear fold of change > 1.3 or < − 1.3 (where minus sign indicates down regulation); the gene's normalized expression signal (in log2 scale) in at least one of the samples was > 5. Expression of several important genes was further verified by RT-PCT in the presence or absence of NN (50 μM): (**B**) stress response gene (**C**) motility-associated genes. Expression of the house-keeping gene, *proC*, was used as the internal control for each sample. Asterisks represent significant differences (***$P < 0.0001$)

aeruginosa resulted in more pronounced differences in the gene expression patterns when compared with those of the control. A clear and remarkable separation was observed in the treatment with NN but not in that with DIV. Interestingly, a comparison of the genes that were differentially expressed after exposure to NN and DIV revealed a minor overlap. Only three genes were exclusively differentially expressed when comparing the effect of DIV to the control. Attenuation of regulation pathways was further verified by the transcriptional analysis. These results allowed us to ascertain that following exposure to NN, the downregulated genes included those that control flagellar motility and pilli formation, genes that specifically affect motility and the ability of the bacteria to form biofilm [51, 52]. Furthermore, qRT-PCR was employed to verify the expression of selected genes. Motility associated genes (pilA, pilG, fliA, and fliG) and survival protein PA4352, a member of the universal stress protein (Usp) superfamily [53], were all significantly downregulated (Fig. 6B, C). The bacteria-bacteria communication signaling systems (QS) regulatory mechanism plays an important role in biofilm development and virulence attack by pathogenic gram-negative bacteria, including *P. aeruginosa* [54]. To elucidate the regulation pathway bisindoles may affect different key regulators, including those of the QS, were screened in the differentiated gene expression maps. Surprisingly, none of the interconnected QS systems, i.e., as, rhl or pqs, were affected by these compounds, indicating that other factors were at play. The attenuation of virulence, biofilm formation, and antibiotic resistance may therefore occur through secondary regulation or further downstream. This may indicate that DIV and NN may have wider ranging effects than we hypothesized. This assumption is supported by the observation that the marine bacteria-derived bisindoles tested here also affected the biofilms of other gram-negative bacteria species (Additional file 1: Fig. 1S).

One possible target of the bisindole compounds is RpoS (σS), a master regulator of the general stress response, which allows differential bacterial survival and adaptation under a variety of stressful conditions [55, 56]. This regulator governs the expression of a large subset of QS-controlled genes at the onset of the stationary phase, including those required for the synthesis of virulence

factors. The reduced expression of RpoS observed following NN treatment is in the line with the findings of virulence and biofilm attenuation (Figs. 1, 2, 3, 4 and 5). In agreement with this, it was shown that the rpoS mutant forms a considerably thinner biofilm, indicating that the RpoS exerts positive feedback on biofilm formation [57]. The ability of these bisindole compounds to disrupt the transcription of a number of factors that are necessary for adhesion and biofilm construction may therefore provide an important new tool to combat the bacterial pathogens that form biofilms.

An important effect of NN and DIV directly on human health is exemplified with the effect on biofilm-growing *P. aeruginosa* in CF patient lungs. There was a downregulation of survival proteins, including PA4352, following exposure of the bacteria to either compound (had FDR *p*-value < 0.05). Downregulation of PA4352 by NN was generally more effective than by DIV. Since this protein may aid in bacterial survival in anaerobic conditions, this result may explain why anaerobic environments, such as the mucus of CF patients, may contribute to the formation of robust biofilms and to increased antibiotic tolerance that together foster the persistence of infections in these patients. Therefore, disruption of homeostatic persistence due to mucoid biofilm-growing *P. aeruginosa* in the CF lungs may retard and even prevent chronic infections [58]. Thus, these compounds may provide an alternative treatment strategy to the use of antibiotics alone. This constitutes an important new defense mechanism in today's post antibiotic era.

To gain a broader comprehension of the possible mechanism of action responsible for sensitizing bacterial virulence properties following NN treatment, a protein network interactions analysis was constructed. The differentially downregulated genes were classified into functional groups using the David database. We further explored the relevant functional clusters by employing STRING analysis (Fig. 7). The selected genes were separated into 4 k-Means clusters. Cluster 1 is composed primarily of the 10 genes that are associated with the regulation of flagellum-dependent cell motility. Cluster 2 comprises biofilm formation related genes. Both of these clusters presented more elaborated evidence network. Cluster 3 contains survival genes (Usp) and cluster 4 is

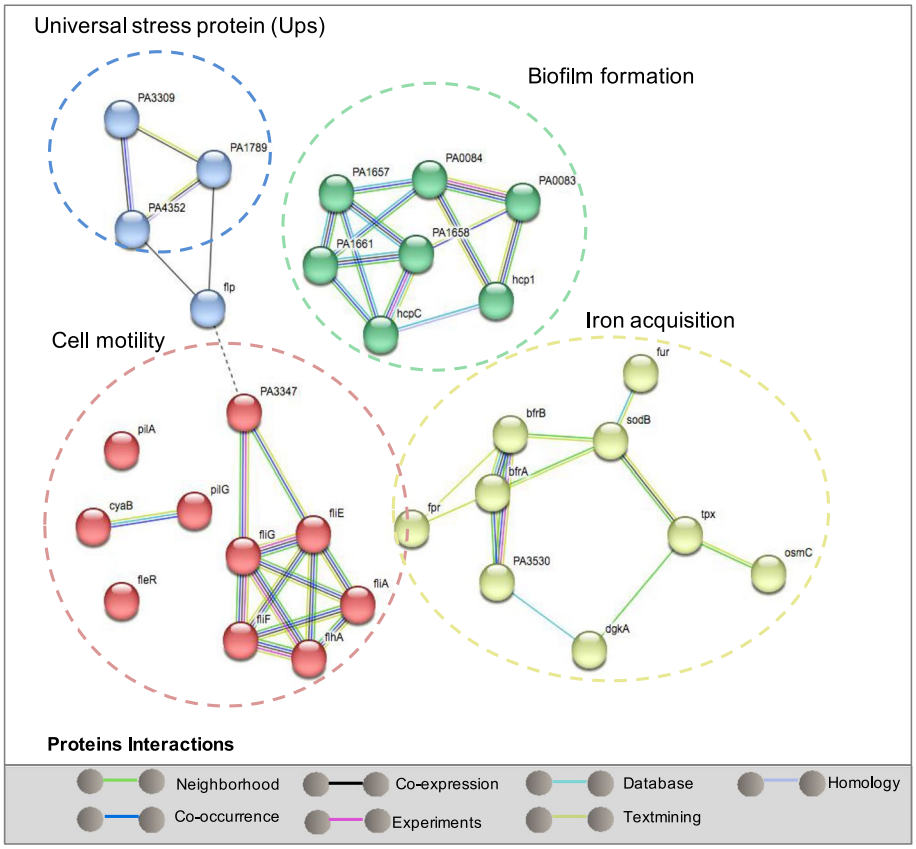

Fig. 7 A STRING cluster interactions network of 30 downregulated genes that were selected based on their functional classification. The identified clusters are colored in red (Cell motility), green (Biofilm formation), yellow (Iron acquisition), and blue (Universal stress protein). The solid and dotted lines indicate connection within the same and different clusters, respectively. Colors indicate the different types of interactions

associated with iron scavenging. In the context of the latter cluster, iron, an indispensable component of many metalloenzymes that support bacterial cell growth and metabolism, is essential for most pathogens [59]. In addition, iron is a critical factor in the transformation of free-living, planktonic *P. aeruginosa* to a sessile, anchored biofilm during all of the biofilm development stages, from adherence to maturation [60]. Under iron limitation, motility is greatly induced, while the incrementally higher levels of iron typical in the sputum of CF patients promotes the non-motile form, the result of which is bacterial aggregation and biofilm formation [61]. Since iron is also quenched by the heme molecule or by circulating proteins such as transferrin or lactoferrin in the host, *P. aeruginosa* circumvents the low iron availability by producing a variety of extracellular chelating molecules [62]. Gene expression STRING analysis indicated that NN downregulated pathways that were related to iron acquisition, and therefore, given the importance of iron for biofilm formation, iron uptake is a possible target of the mode of action of NN.

Conclusions

We identified indole-based compound in coral-associated bacteria that possess anti-biofilm and anti-virulence properties. These molecules can be effective candidates for cases in which antibiotic treatment alone may potentially foster the development of a resistant chronic infection via the establishment of a resistant biofilm. The use of these marine microbiome bisindole-based compounds may be a viable strategy to eradicate biofilm-associated pathogens. Indeed, our results indicate that such an integration of conventional antibiotic treatment together with bisindole can be developed into a novel, advanced system for the generation of new drug combination therapeutics to reduce the dangers to human health posed by antibiotic-resistant pathogens. Combining natural sources and synthetic methods can significantly accelerate drug discovery and development. A multidisciplinary approach is essential in identifying new molecular structures and biosynthetic pathways, thereby expanding the database of natural products. The increasing trend of digitization in the field of chemistry will further aid in this endeavor by providing researchers with a vast array of nature-inspired chemicals for generative modeling and high-throughput screening. Through the utilization of natural product libraries, drug discovery can become more cost-effective, as it reduces financial and resource requirements while providing a large pool of potential drug candidates. This approach will fully unleash the potential of both natural products and synthetic methodologies, leading to the ultimate goal of improving human health.

Materials and methods

Extraction and purification of active compounds

Bacterial isolate associate with the stony *Favia* sp., coral was collected from a reef adjacent to the Inter-University Institute for Marine Science in the Gulf of Eilat, Israel. The sample was obtained from the coral mucus layer. To obtain a sample of coral-associated bacterial cell culture, a 230-ml volume was extracted twice with equal volumes of dichloromethane. The resulting organic phase was concentrated using a rotary evaporator under vacuum to reduce the volume to 25 ml. This was followed by evaporation to dryness using a continuous flow of nitrogen. The residue of each batch was then resuspended in a mixture of 173 µl of ethyl acetate acidified with formic acid (0.5% (v/v)) and 27 µl of acetonitrile. The total extract volume of 200 µl was added to 3 ml of thrice-distilled water with approximately 200 µl of acetonitrile. This mixture was then centrifuged at 4000 rcf for 5 min and subjected to a round of preparative high-performance liquid chromatography (HPLC). After obtaining the active fraction, we proceeded to further purify it using two distinct protocols. The first purification protocol involved the use of reversed-phase preparative HPLC (Thermo Spectra Physics), a C18 column, and a linear water/acetonitrile gradient containing 0.1% TFA at a flow rate of 1 ml/min and monitored at 260 nm. The peak was successfully eluted at approximately 18 min.

To ensure the purity of the fraction, we subjected it to analytical HPLC (Dionex 1100) with a C18 column, an injection volume of 30 µl, and a linear water/acetonitrile gradient containing 0.1% TFA, ranging from 20 to 50% at a rate of 2.5%/min. Subsequently, we collected the fraction and lyophilized it, and the residue was dissolved in 1 ml of 1:1 (v/v) acetonitrile/water.

To determine the molecular weight of the purified fraction, we utilized mass spectrometry (MS) on a LTQ XL Orbitrap with static nanospray (Thermo-Fisher, San Jose, CA) in positive ion mode. The fraction was identified as NN. For the second purification protocol, normal normal-phase HPLC was utilized with the same conditions mentioned earlier for the reversed-phase preparative HPLC. The elution of the peak occurred around 4 min. To ensure the purity of the peak, analytical HPLC was performed. The collected fraction was lyophilized, and the residue was dissolved in 1 ml of 1:1 (v/v) acetonitrile/water to determine the molecular weight in positive ion mode. This particular fraction corresponds to DIV. To summarize the findings, the fractions NN and DIV were successfully identified and their structures were determined through precise spectral analysis using UV, LC/MS, MS, and NMR techniques. The NMR spectra were recorded on a Bruker AVANCE 300, operating at 300 MHz for 1H. LC/MS was carried out on a Waters

Alliance 2695-ZQ2000 with a column X-Bridge C18 4.5 ×150 mm, 5 µm, and detected through UV and corona detection. ESI mass spectra were obtained with a Waters micromass ZQ 2000 mass spectrometer. The absorption spectra of the purified fractions NN and DIV were obtained using a photodiode array detector.

NN synthesis

For the *NN* synthesis, a solution of $[(Me_3Si)_2N]_3RE(\mu\text{-}Cl)Li(THF)_3$ (1.3 mmol), indole (1 mmol), and THF (10 mL) was prepared using a 30-mL schlenk tube under a schlenk line. The mixture was stirred at room temperature for 15 min, followed by an additional 20 min of stirring in the air atmosphere. Next, a diluted hydrochloric acid solution (0.1 M, 2 mL) was added, and the resulting solution was extracted with diethyl ether, dried using anhydrous magnesium sulfate, and filtered. The solvents were then evaporated, and the remaining residue was purified using a silica gel column chromatography. By using a mixture of n-hexane and ethyl acetate (30:1, v/v) as an eluent, a red solid, identified as 1,1'-bisindole, was obtained with a yield of 35%.

^{1}H-NMR δ 7.73 (dd, J = 23.6, 5.5 Hz, 1H), 7.32 (d, J = 3.3 Hz, 1H), 7.20 (t, J = 6.9 Hz, 1H), 7.16 (t, J = 7.6 Hz, 1H), 6.89 (d, J = 7.9 Hz, 1H), 6.67 (d, J = 3.1 Hz, 1H).

^{1}H-NMR (DMSO, 400 MHz) δ 7.7 (m, 4H), 7.1 (m, 4H,), 6.7 (m, 4H).

^{13}C NMR (400 MHz, $CDCl_3$) δ 136.8, 127.9, 126.2, 123.2, 121.3, 121.2, 109.0, 102.2.

^{13}C NMR (400 MHz, DMSO) δ 136.7, 129.5, 126.4, 123.5, 121.7, 121.4, 108.8, 102.3.

EI-MS m/z calculated for $C_{16}H_{12}N_2$ [M + H]: 233.0078, found: 233.1.

DIV synthesis

According to the procedure previously described by Somei, the desired product was obtained.

^{1}H-NMR (DMSO 400 MHz) δ 3.1 (1 H, dd, J = 154 and J = 9.2 Hz), 3.7 (1 H, dd, J = 15.4 and 9.2 Hz), 5.8 (1 H, dt, J = 2.7 and 9.2 Hz), 6.0 (1 H, d, J = 2.7 Hz), 6.3 (1 H, d, J = 2.2 Hz), 6.5 (1 H, ddd, J = 7.3, 6.5, and 1.0 Hz), 6.5 (1H, d, J = 7.3 Hz), 6.9 (1H, ddd, J = 7.3, 6.5, and 1.0 Hz), 6.9 (1H, t, J = 7.3 Hz), 7.0 (1H, ddd, J = 7.3, 6.5, and 1.0 Hz), 7.04 (1H, d, J = 7.3 Hz), 7.3 (1H, dd, J = 7.3 and l.0 Hz), 7.4 (1H, d, J = 7.3 Hz), 11.05 (1H, br s).

^{13}C NMR (DMSO 400 MHz): δ 140.0, 130.0, 128.0, 127.8, 125.6, 125.3, 124.5, 122.6, 122.0, 120.0, 118.9, 118.3, 116.7, 111.5, 59.8, 38.0.

EI-MS m/z: 235 $(M + H)^+$.

Bacterial strains and culture conditions

Four gram-negative biofilm-forming pathogens, *Pseudomonas aeruginosa* PA01, *Acinetobacter baumannii*, *Serratia marcescens*, and *Providencia stuartii* strains, were grown at 37 °C in LB medium (Difco Luria–Bertani medium, BD, France) with constant agitation at 120 rpm for 24 h. The active compounds were extracted from coral-associated bacteria grown at 26 °C in marine broth (Himedia Laboratories, Mumbai, India). All the bacteria used in this study are from our laboratory collection.

Development of a biofilm formation assay under static conditions

To test for the efficacy of the compounds against biofilms, prevention tests in short-term static biofilm models were employed to study the early steps of biofilm formation by *A. baumannii*, *S. marcescens*, *P. stuartii*, and *P. aeruginosa*. Overnight cultures of the test strains were diluted 1:10 into modified 10% (w/v) LB medium supplemented with 0.56 mM glucose and 50 µM of either NN or DIV or an equivalent concentration of DMSO and incubated at 37 °C with agitation at 120 rpm until it reached the middle-exponential growth phase (OD600 ~0.5). Glass-bottom microtiter plates containing 96 wells (Thermo Fisher) with 200 µl of modified LB medium, 50 µM NN or DIV, and 1% re-grown biofilm model bacterial strain per well were statically incubated at 37 °C. After 24 h, the resulting biofilms were macroscopically visualized using the LIVE/DEAD *Bac*Light viability staining kit (Molecular Probes Inc., Eugene, OR) according to the manufacturer's instructions. The SYTO 9 stained live cells and the PI stained dead ones, as was determined by CSLM.

Microscopy and image analysis

The developing biofilms were visualized in situ using CLSM, FV1000 (Olympus, Tokyo, Japan) equipped with a 60 ×1.35 NA lens. Image scanning was carried out using the 488 and 541 nm lasers for the detection of SYTO 9 and PI, respectively. The excitation wavelength for the green-live dye was 488 nm and emission was collected using a 505–525 band pass filter; for the red-dead PI stain, the excitation was 541 nm and emission was collected using a 560–660 band pass filter. Simulated fluorescence projections of the biofilm-stacks were used to reconstruct the 3D biofilm architecture using Imaris software (Bitplane AG, Zu¨rich, Switzerland). Additionally, a quantitative structural parameter for biovolumes ($\mu m^3/\mu m^2$) was calculated with Imaris Measurement Pro.

Continuous-culture biofilm flow chamber system

The developing biofilms were monitored in a continuous flow-cell system, assembled, and prepared as described previously [63]. To follow biofilm destruction, *P. aeruginosa* PA01 was allowed to form a biofilm in a flow chamber for 72 h before 50 µM NN and 20 µg/ml tobramycin were introduced. *P. aeruginosa* was cultivated in flow

chambers supplied with AB trace minimal medium containing 0.3 mM glucose. The flow cell was inoculated with an overnight culture diluted with 0.9% NaCl to an OD_{595} of 0.1. After inoculation, flow was turned off for 1 h to allow initial bacteria attachment to the substratum of the microscope glass coverslip. Thereafter, the medium was continually pumped at a constant rate of 3 ml h^{-1} at 37 °C for the duration of the experiment using a Masterflex L/S peristaltic pump (Cole-Parmer, Illinois, USA). Afterwards, biofilms were stained with LIVE/DEAD *Bac*Light bacterial viability staining and their thicknesses were measured and assessed using a CLSM and the IMARIS software.

Tobramycin was chosen in light of the screening results of several antibiotics, including gentamicin, tobramycin, azithromycin, levofloxacin, ciprofloxacin, and colistin, using the minimum inhibitory concentration (MIC) assay as determined by E-TEST (Biomérieux). Gradient concentration strips were placed on a lawn of *P. aeruginosa* that formed on 1% Mueller–Hinton agar plates (Himedia Laboratories) supplemented with either 50 µM NN or 50 µM DIV. MIC values were evaluated after incubation for 24 h at 37 °C.

Quantification of extracellular virulence factor production by *P. aeruginosa* PA01

An overnight culture of *P. aeruginosa* PAO1 was diluted to a fresh LB medium (1:600) supplemented with 50 µM of either NN or DIV and incubated at 37 °C with agitation for 24 h. The virulence factors of *P. aeruginosa* PAO1 cell-free culture (centrifuged for 15 min at 3700 rpm) were quantified as previously described [64, 65]. Production of *pyocyanin* was measured by extracting the pigment from 4 ml of cell-free culture with chloroform at a ratio of 3:2 by gently shaking the phases; the blue pigmentation of the chloroform corresponded to the pyocyanin. This was followed by a second extraction of the organic phase with 800 µl of 0.2 M HCl. Absorbance was measured at OD 540 nm. For the *pyoverdine* assay, the concentration was measured by using the characteristic absorbance at 380 nm. *Elastase* activity of LasB was determined by the method of Sarabhai et al. [64]. Briefly, elastin-congo red (5 mg ml^{-1}) (Sigma) in 0.1 M Tris–HCl buffer (pH 8; 1 mM $CaCl_2$) was added to cell-free culture at a ratio of 3:1 and incubated for 1 week at 37 °C with agitation at 200 rpm. After centrifugation (6000 *g* for 10 min), the absorbance was read at 400 nm. *Lipase* activity was assessed by mixing 0.3 ml of cell-free culture with 0.3 ml Tween 20 in Tris-buffered saline (10%), 50 µl of $CaCl_2$ (1 M), and 0.6 ml of double-distilled water followed by 24 h of incubation at 37 °C with agitation at 200 rpm. The turbidity of this solution was measured at OD 400 nm because lipase breaks down Tween, and the resulting compound, in turn, binds to calcium and precipitates. *Rhamnolipids* were quantified by acidification of the supernatant with concentrated HCl 10 M until it reached pH 2, after which the acidic suspension was centrifuged at 8000 *g* for 10 min and the absorbance was measured at OD 570 nm. Total *protease* activity was estimated using azocasein as a substrate by modification of the method [66]. The assay mixture was prepared in a reaction volume of 400 µl that contained 0.8% azocasein (Sigma) in phosphate-buffered saline (pH 7) and cell-free culture at a ratio of 1:1. After static incubation at 37 °C for 1 h, the reaction was stopped by the addition of 500 µl trichloroacetic acid (10%), and the mixture was then centrifuged at 8000 *g* for 5 min to precipitate residual azocasein. The absorbance was determined at 400 nm. To determine *chitinase* activity, 0.5 ml of cell-free culture was added to 2.5 mg of insoluble chitin-azure (Sigma) and 0.5 ml PBS. The mixture was then incubated for 24 h at 37 °C with agitation at 200 rpm. The insoluble chitin-azure was removed by centrifugation at 16,000 *g* for 10 min, and the absorbance was measured at OD 570 nm. A sub-inhibitory concentration of tetracycline 0.6 µg/ml served as controls.

Caenorhabditis elegans paralytic assay

To assess the toxicity of these compounds on eukaryotes, a nematode toxicity assay was used. The N2 wild-type hermaphrodite strain of the nematode *C. elegans* (Bristol) was grown on NGM plates seeded with the *Escherichia coli* OP50 strains at 15 °C. L4 stage worms were removed and transferred to a 24-well plate containing M9 medium (100 mM Tris–HCl, pH 7.4, 17 mM NaCl), 1% cholesterol, 30 mM glucose, and 5 µM SYTOX Orange. This mixture was supplemented with 50 µM [1,1'-bisindole (NN) and 2,3-dihydro-2,2'-bisindole (DIV)] or an equivalent volume of DMSO. Approximately 20–25 nematodes (L4) were placed into each well together with 1×10^8 *P. aeruginosa* PAO1 and incubated at 25 °C. Worms were evaluated for viability every 2 h over a total elapsed time of 24 h. Survival was scored by assessment of either dye uptake using a Leica M165 FC fluorescent stereoscope or non-response to physical stimuli [67].

P. aeruginosa PA01 adhesion to A549 human lung cell assay

The A549 epithelial cells (lung adenocarcinoma cells; ATCC, Rockville, MD, USA) were seeded in 96-well plates at 25×10^4 cells per ml in 200 µl of Dulbecco's modified Eagle's medium (DMEM) supplemented with 10% fetal calf serum (FCS) (pH 7.1) at 37 °C under 5% CO_2 and grown to a 100% confluent monolayer. After 24 h, the growth medium was replaced with DMEM supplemented with 1% gelatin to block non-specific binding sites. A549 cells were infected with *P. aeruginosa*

PA01 that had been grown overnight with either 50 μM [1,1'-bisindole (NN) and 2,3-dihydro-2,2'-bisindole (DIV)] or with an equivalent amount of DMSO. *P. aeruginosa*-human cell interactions were ascertained by assessing the adherence potential of the bacteria to the cells. After blocking, A549 cells were infected with *P. aeruginosa* PA01 in multiplicity of infection (MOI) of 40 followed by incubation for 1 h at 37 °C in 5% CO_2. PBS washes were used to remove non-adhered bacteria, and the adhered cells were then released by treatment with 0.25% trypsin–EDTA and plated in serial dilution onto LB agar plates for the enumeration of adherent bacterial cells.

Cytotoxic effect and apoptosis of A549 human lung cells

A549 cells were washed twice with PBS buffer, then serum-free DMEM was added, and the well-plates were incubated for 2 h at 37°C. Cells were subsequently infected with *P. aeruginosa* PA01. For inoculation, the overnight *P. aeruginosa* PA01 culture was pelleted by centrifugation and diluted into an equivalent volume of fresh LB broth to allow it to grow for approximately 2 h. The bacteria pellet was washed once in PBS buffer and then resuspended in DMEM medium to a concentration of 5×10^7 CFU/ml. Bacterial dilution was then added to the A549 cell monolayers at MOI of 40, to which was added either 50 μM 1,1'-bisindole (NN) or 2,3-dihydro-2,2'-bisindole (DIV)] and as a control, an equivalent volume of DMSO and the serum-free DMEM was replaced with complete DMEM. At the indicated time point of incubation at 37 °C under 5% CO_2, A549 cell viability was assessed using Calcein AM (ThermoFisher) according to the manufacturer's instructions and the Operetta high-throughput fluorescent microscope system (Perkin-Elmer, Hamburg, Germany). In each well, 20 fields were imaged using a × 20 wide-field objective with an excitation filter of 520–550 nm and an emission filter of 560–630 nm.

RNA preparation for DNA microarray analysis

Overnight cultures of *P. aeruginosa* PAO1 were diluted 1:600 into fresh LB medium following supplementation of equivalent volumes of 50 μM of NN, DIV, or DMSO as a control for additional growth at 37 °C under agitation. Samples were retrieved after 18 h, and two volumes of RNAprotect Bacteria reagent were added (Qiagen). RNA was extracted using the RNeasy Mini kit (Qiagen), including on-column digestion with RNase-free DNase I (Qiagen) in accordance with the manufacturer's instructions. RNA was isolated using the RNeasy mini-purification kit (Qiagen) with on-column DNase treatment. The whole transcriptome of *P. aeruginosa* was amplified using the senationPlus FFPE amplification kit of Affymetrix. Essentially, total RNA purified from *P. aeruginosa* cells was reverse transcribed using random primers. Poly (dA) were then tailed onto the 3'ends of the transcribed cDNA using dATP and terminal deoxynucleotidyl transferase. An oligonucleotide comprising T7 promoter and poly (dT) was hybridized to the Poly (dA) region of the cDNA, and Klenow polymerase was used to generate a double-stranded T7 promoter region on the single-stranded cDNA. The amplified amounts of senseRNA were transcribed by using T7 RNA polymerase and a NTP mix. The senseRNA was subsequently used to reverse transcribe the single-stranded cDNA that had been fragmented and end-labeled at the 3′ ends with biotin. These single stranded cDNA fragments were then used to hybridize the *P. aeruginosa* genome arrays (Affymetrix) according to the manufacturer's instructions. Microarray data analysis was carried out using the Partek® Genomics Suite. Affymetrix CEL files of Pae-G1a arrays were loaded into Partek and preprocessed using RMA and quantile normalization. Normalized expression signals were reported in log2 scale. Prior to clustering, the Partek Batch Remover method was applied to the expression signals to correct for the batch effect. The signals were then standardized so that for each gene the mean was shifted to zero and the standard deviation was scaled to 1. The hierarchical clustering used Pearson's dissimilarity as the distance measure and complete linkage for cluster-distance estimation. To identify differentially expressed genes, a 2-way ANOVA was carried out, with the treatment as fixed effect and the batch as random effect. The contrasts (pairwise comparisons) DIV vs. DMSO and NN vs. DMSO were included in the ANOVA model following adjustment for multiple testing using the FDR method. Based on pathway analyses by David Bioinformatics resources, we conducted a protein interactions analysis using the STRING database, version 11.5. The interacting proteins were clustered using Markov clustering based on the Gene Ontology biological process and the Kyoto Encyclopedia of Genes and Genomes KEGG pathway.

Reverse transcription and real-time PCR

RNA extractions were performed as described above. cDNA was prepared using One Step PrimeScript RT Master Mix (TAKARA). Expression of the *P. aeruginosa* PA01 target genes *proC* (PA0393), *pilA* (PA4525), *pilG* (PA0408), *fliA* (PA1455), *fliG* (PA1102), and *PA4352* genes was evaluated using RT-qPCR. Primers used for qRT-PCR are listed in Additional File 1: Table 2S. Amplification was executed using the Step One Plus real-time PCR 110 system (Applied Biosystems, Thermo Scientific). Duplicate PCR reactions were performed using the qPCRBIO SyGreen Blue Mix Hi-ROX (PCR Biosystems).

The reaction involved 15 min of activation of the modified Taq polymerase at 95 °C, 40 cycles of 15 s at 95 °C and 1 min at 60 °C. A melt curve was run at the end of the 40 cycles to test for the presence of a unique PCR reaction product. *proC* was used as an internal reference.

Statistical analysis

The statistical methods, which were applied for the anti-biofilm or anti-virulence experiments used either one-way ANOVA with Tukey's test or *T*-test taking into account 3–6 replicates.

Abbreviations

NN	1,1'-Bisindole
DIV	2,3-Dihydro-2,2'-bisindole
WHO	World Health Organization
QS	Quorum sensing
IPA	Indole-3-propionic acid
CSLM	Confocal scanning laser microscopy
PI	Propidium iodide
MOI	Multiplicity of infection

Supplementary Information

The online version contains supplementary material available at https://doi.org/10.1186/s12915-025-02234-7.

Additional file 1: Figure 1S. Effect of NN on biofilm formation by *P. stuartii* and *S. marcescens* in static growth mode. Figure 2S. Preprocessing of the microarray results. Table 1S. Antimicrobial susceptibility tests. Table 1S. Primers list for qRT-PCR.

Acknowledgements

The authors would like to thank Levi Eshkol scholarship from the Israeli Ministry of Science and Technology; Shimona Geresh award and Avram and Stella Goldstein-Goren fund for partial support. The authors also thank Prof. Gonen Ashkenasy, Prof. Doron Pappo, and Dr. Amira Rudi for their guidance and their help with chemical work. + This paper is dedicated to the memory of Prof. Yaffa Mizrachi Nebenzahl, who also participated in this study.

Authors' contributions

Conceptualization: KG, YMN, ABZ, RM, AK. Methodology: KG. Investigation: KG, BK, MS, NS. Data analysis: KG, KE. Writing: KG, KE, EKW. Funding acquisition: AK, RM. Supervision: YMN, AK, RM. All authors read and approved the final manuscript.

Funding

This work was supported by the National Institute of Biotechnology in the Negev (NIBN), with financial support under grant number 8528620 "Bioactive compounds."

Data availability

All data generated or analyzed during this study are included in this published article and its supplementary information file. The strains, reagents, and datasets used and/or analyzed during the current study are available from the corresponding author on reasonable request.

Declarations

Ethics approval and consent to participate

Not applicable.

Consent for publication

Not applicable.

Competing interests

The authors declare that they have no competing interests.

Received: 26 March 2024 Accepted: 5 May 2025
Published online: 15 May 2025

References

1. Romandini A, Pani A, Schenardi PA, Pattarino GAC, De Giacomo C, Scaglione F. Antibiotic resistance in pediatric infections: global emerging threats, predicting the near future. Antibiotics. 2021;10(4):393.
2. Church NA, McKillip JL. Antibiotic resistance crisis: challenges and imperatives. Biologia. 2021;76(5):1535–50.
3. Aslam B, Wang W, Arshad MI, Khurshid M, Muzammil S, Rasool MH, Nisar MA, Alvi RF, Aslam MA, Qamar MU. Antibiotic resistance: a rundown of a global crisis. Infect Drug Resist. 2018;11:1645–58.
4. La Rosa R, Johansen HK, Molin S. Persistent bacterial infections, antibiotic treatment failure, and microbial adaptive evolution. Antibiotics. 2022;11(3):419.
5. Young D, Hussell T, Dougan G. Chronic bacterial infections: living with unwanted guests. Nat Immunol. 2002;3(11):1026–32.
6. Vestby LK, Grønseth T, Simm R, Nesse LL. Bacterial biofilm and its role in the pathogenesis of disease. Antibiotics. 2020;9(2):59.
7. Jamal M, Ahmad W, Andleeb S, Jalil F, Imran M, Nawaz MA, Hussain T, Ali M, Rafiq M, Kamil MA. Bacterial biofilm and associated infections. J Chin Med Assoc. 2018;81(1):7–11.
8. Flemming H-C, Wingender J, Szewzyk U, Steinberg P, Rice SA, Kjelleberg S. Biofilms: an emergent form of bacterial life. Nat Rev Microbiol. 2016;14(9):563–75.
9. Gebreyohannes G, Nyerere A, Bii C, Sbhatu D. Challenges of intervention, treatment, and antibiotic resistance of biofilm-forming microorganisms. Heliyon. 2019;5(8):e02192.
10. Moser C, Pedersen HT, Lerche CJ, Kolpen M, Line L, Thomsen K, Høiby N, Jensen PØ. Biofilms and host response–helpful or harmful. APMIS. 2017;125(4):320–38.
11. Exner M, Bhattacharya S, Christiansen B, Gebel J, Goroncy-Bermes P, Hartemann P, Heeg P, Ilschner C, Kramer A, Larson E. Antibiotic resistance: What is so special about multidrug-resistant Gram-negative bacteria? GMS Hyg Infect Control. 2017;12:Doc05.
12. Koulenti D, Song A, Ellingboe A, Abdul-Aziz MH, Harris P, Gavey E, Lipman J. Infections by multidrug-resistant Gram-negative Bacteria: What's new in our arsenal and what's in the pipeline? Int J Antimicrob Agents. 2019;53(3):211–24.
13. Abisado RG, Benomar S, Klaus JR, Dandekar AA, Chandler JR. Bacterial quorum sensing and microbial community interactions. MBio. 2018;9(3):e02331-17. https://doi.org/10.1128/mbio.02331-02317.
14. Preda VG, Săndulescu O. Communication is the key: biofilms, quorum sensing, formation and prevention. Discoveries. 2019;7(3):e100.
15. Mukherjee S, Bassler BL. Bacterial quorum sensing in complex and dynamically changing environments. Nat Rev Microbiol. 2019;17(6):371–82.
16. Saeki EK, Kobayashi RKT, Nakazato G. Quorum sensing system: Target to control the spread of bacterial infections. Microb Pathog. 2020;142:104068.
17. Azimi S, Klementiev AD, Whiteley M, Diggle SP. Bacterial quorum sensing during infection. Annu Rev Microbiol. 2020;74:201–19.
18. Melander RJ, Basak AK, Melander C. Natural products as inspiration for the development of bacterial antibiofilm agents. Nat Prod Rep. 2020;37(11):1454–77.
19. Marchese P, Young R, O'Connell E, Afoullouss S, Baker BJ, Allcock AL, Barry F, Murphy JM. Deep-sea coral garden invertebrates and their associated fungi are genetic resources for chronic disease drug discovery. Mar Drugs. 2021;19(7):390.
20. Leal MC, Calado R, Sheridan C, Alimonti A, Osinga R. Coral aquaculture to support drug discovery. Trends Biotechnol. 2013;31(10):555–61.
21. Golberg K, Pavlov V, Marks RS, Kushmaro A. Coral-associated bacteria, quorum sensing disrupters, and the regulation of biofouling. Biofouling. 2013;29(6):669–82.

22. Rasmussen TB, Givskov M. Quorum-sensing inhibitors as anti-pathogenic drugs. Int J Med Microbiol. 2006;296(2–3):149–61.
23. Mishra R, Panda AK, De Mandal S, Shakeel M, Bisht SS, Khan J. Natural anti-biofilm agents: strategies to control biofilm-forming pathogens. Front Microbiol. 2020;11:566325.
24. Lu L, Hu W, Tian Z, Yuan D, Yi G, Zhou Y, Cheng Q, Zhu J, Li M. Developing natural products as potential anti-biofilm agents. Chin Med. 2019;14(1):1–17.
25. Solanki R, Khanna M, Lal R. Bioactive compounds from marine actinomycetes. Indian J Microbiol. 2008;48:410–31.
26. Ameen F, AlNadhari S, Al-Homaidan AA. Marine microorganisms as an untapped source of bioactive compounds. Saudi J Biol Sci. 2021;28(1):224–31.
27. Ma Z-P, Song Y, Cai Z-H, Lin Z-J, Lin G-H, Wang Y, Zhou J. Anti-quorum sensing activities of selected coral symbiotic bacterial extracts from the South China Sea. Front Cell Infect Microbiol. 2018;8:144.
28. Golberg K, Eltzov E, Shnit-Orland M, Marks RS, Kushmaro A. Characterization of quorum sensing signals in coral-associated bacteria. Microb Ecol. 2011;61:783–92.
29. Wibowo JT, Ahmadi P, Rahmawati SI, Bayu A, Putra MY, Kijjoa A. Marine-derived indole alkaloids and their biological and pharmacological activities. Mar Drugs. 2021;20(1):3.
30. Lott JS. The tryptophan biosynthetic pathway is essential for Mycobacterium tuberculosis to cause disease. Biochem Soc Trans. 2020;48(5):2029–37.
31. Li X, Zhang B, Hu Y, Zhao Y. New insights into gut-bacteria-derived indole and its derivatives in intestinal and liver diseases. Front Pharmacol. 2021;12:769501.
32. Wilson ZE, Brimble MA. Molecules derived from the extremes of life. Nat Prod Rep. 2009;26(1):44–71.
33. Gillespie DE, Brady SF, Bettermann AD, Cianciotto NP, Liles MR, Rondon MR, Clardy J, Goodman RM, Handelsman J. Isolation of antibiotics turbomycin A and B from a metagenomic library of soil microbial DNA. Appl Environ Microbiol. 2002;68(9):4301–6.
34. Lee J-H, Wood TK, Lee J. Roles of indole as an interspecies and interkingdom signaling molecule. Trends Microbiol. 2015;23(11):707–18.
35. Liu HB, Lee JH, Kim JS, Park S. Inhibitors of the Pseudomonas aeruginosa quorum-sensing regulator. QscR Biotechnol Bioeng. 2010;106(1):119–26.
36. Yan J, Bassler BL. Surviving as a community: antibiotic tolerance and persistence in bacterial biofilms. Cell Host Microbe. 2019;26(1):15–21.
37. Taccetti G, Francalanci M, Pizzamiglio G, Messore B, Carnovale V, Cimino G, Cipolli M. Cystic fibrosis: Recent insights into inhaled antibiotic treatment and future perspectives. Antibiotics. 2021;10(3):338.
38. Golberg K, Markus V. Kagan B-e, Barzanizan S, Yaniv K, Teralı K, Kramarsky-Winter E, Marks RS, Kushmaro A: Anti-Virulence Activity of 3, 3′-Diindolylmethane (DIM): A Bioactive Cruciferous Phytochemical with Accelerated Wound Healing Benefits. Pharmaceutics. 2022;14(5):967.
39. Luo J, Dong B, Wang K, Cai S, Liu T, Cheng X, Lei D, Chen Y, Li Y, Kong J. Baicalin inhibits biofilm formation, attenuates the quorum sensing-controlled virulence and enhances Pseudomonas aeruginosa clearance in a mouse peritoneal implant infection model. PLoS ONE. 2017;12(4):e0176883.
40. Brackman G, Hillaert U, Van Calenbergh S, Nelis HJ, Coenye T. Use of quorum sensing inhibitors to interfere with biofilm formation and development in Burkholderia multivorans and Burkholderia cenocepacia. Res Microbiol. 2009;160(2):144–51.
41. Brackman G, Cos P, Maes L, Nelis HJ, Coenye T. Quorum sensing inhibitors increase the susceptibility of bacterial biofilms to antibiotics in vitro and in vivo. Antimicrob Agents Chemother. 2011;55(6):2655–61.
42. Rezzoagli C, Archetti M, Mignot I, Baumgartner M, Kümmerli R. Combining antibiotics with antivirulence compounds can have synergistic effects and reverse selection for antibiotic resistance in Pseudomonas aeruginosa. PLoS Biol. 2020;18(8):e3000805.
43. Jiang P, Li J, Han F, Duan G, Lu X, Gu Y, Yu W. Antibiofilm activity of an exopolysaccharide from marine bacterium Vibrio sp. QY101. PLoS One. 2011;6(4):e18514.
44. Ribet D, Cossart P. How bacterial pathogens colonize their hosts and invade deeper tissues. Microb Infect. 2015;17(3):173–83.
45. Strateva T, Mitov I. Contribution of an arsenal of virulence factors to pathogenesis of Pseudomonas aeruginosa infections. Ann Microbiol. 2011;61(4):717–32.
46. Lau GW, Hassett DJ, Ran H, Kong F. The role of pyocyanin in Pseudomonas aeruginosa infection. Trends Mol Med. 2004;10(12):599–606.
47. Kang D, Revtovich AV, Chen Q, Shah KN, Cannon CL, Kirienko NV. Pyoverdine-dependent virulence of Pseudomonas aeruginosa isolates from cystic fibrosis patients. Front Microbiol. 2019;10:2048.
48. Irazoqui JE, Urbach JM, Ausubel FM. Evolution of host innate defence: insights from Caenorhabditis elegans and primitive invertebrates. Nat Rev Immunol. 2010;10(1):47–58.
49. Ewbank JJ. Signaling in the immune response. WormBook. 2006:1–12.
50. Hawdon NA, Aval PS, Barnes RJ, Gravelle SK, Rosengren J, Khan S, Ciofu O, Johansen HK, Høiby N, Ulanova M. Cellular responses of A549 alveolar epithelial cells to serially collected Pseudomonas aeruginosa from cystic fibrosis patients at different stages of pulmonary infection. FEMS Immunol Med Microbiol. 2010;59(2):207–20.
51. Barken KB, Pamp SJ, Yang L, Gjermansen M, Bertrand JJ, Klausen M, Givskov M, Whitchurch CB, Engel JN, Tolker-Nielsen T. Roles of type IV pili, flagellum-mediated motility and extracellular DNA in the formation of mature multicellular structures in Pseudomonas aeruginosa biofilms. Environ Microbiol. 2008;10(9):2331–43.
52. O'Toole GA, Wong GC. Sensational biofilms: surface sensing in bacteria. Curr Opin Microbiol. 2016;30:139–46.
53. Boes N, Schreiber K, Härtig E, Jaensch L, Schobert M. The Pseudomonas aeruginosa universal stress protein PA4352 is essential for surviving anaerobic energy stress. J Bacteriol. 2006;188(18):6529–38.
54. Saxena P, Joshi Y, Rawat K, Bisht R. Biofilms: architecture, resistance, quorum sensing and control mechanisms. Indian J Microbiol. 2019;59:3–12.
55. Schuster M, Hawkins AC, Harwood CS, Greenberg E. The Pseudomonas aeruginosa RpoS regulon and its relationship to quorum sensing. Mol Microbiol. 2004;51(4):973–85.
56. Lee J, Zhang L. The hierarchy quorum sensing network in Pseudomonas aeruginosa. Protein Cell. 2015;6(1):26–41.
57. Bouillet S, Ba M, Houot L, Iobbi-Nivol C, Bordi C. Connected partner-switches control the life style of Pseudomonas aeruginosa through RpoS regulation. Sci Rep. 2019;9(1):6496.
58. Martin I, Waters V, Grasemann H. Approaches to targeting bacterial biofilms in cystic fibrosis airways. Int J Mol Sci. 2021;22(4):2155.
59. Rajakovich LJ, Balskus EP. Metabolic functions of the human gut microbiota: the role of metalloenzymes. Nat Prod Rep. 2019;36(4):593–625.
60. Zhang Y, Pan X, Wang L, Chen L. Iron metabolism in Pseudomonas aeruginosa biofilm and the involved iron-targeted anti-biofilm strategies. J Drug Target. 2021;29(3):249–58.
61. Berlutti F, Morea C, Battistoni A, Sarli S, Cipriani P, Superti F, Ammendolia M, Valenti P. Iron availability influences aggregation, biofilm, adhesion and invasion of Pseudomonas aeruginosa and Burkholderia cenocepacia. Int J Immunopathol Pharmacol. 2005;18(4):661–70.
62. Cornelis P, Dingemans J. Pseudomonas aeruginosa adapts its iron uptake strategies in function of the type of infections. Front Cell Infect Microbiol. 2013;3:75.
63. Pamp SJ, Sternberg C, Tolker-Nielsen T. Insight into the microbial multicellular lifestyle via flow-cell technology and confocal microscopy. J Int Soc Anal Cytol. 2009;75(2):90–103.
64. Sarabhai S, Sharma P, Capalash N. Ellagic acid derivatives from Terminalia chebula Retz. downregulate the expression of quorum sensing genes to attenuate Pseudomonas aeruginosa PAO1 virulence. PLoS One. 2013;8(1):e53441.
65. Solleti VS, Alhariri M, Halwani M, Omri A. Antimicrobial properties of liposomal azithromycin for Pseudomonas infections in cystic fibrosis patients. J Antimicrob Chemother. 2015;70(3):784–96.
66. Andrejko M, Zdybicka-Barabas A, Janczarek M, Cytryńska M. Three Pseudomonas aeruginosa strains with different protease profiles. Acta Biochim Pol. 2013;60(1):83–90.
67. Shemesh N, Shai N, Ben-Zvi A. Germline stem cell arrest inhibits the collapse of somatic proteostasis early in C aenorhabditis elegans adulthood. Aging Cell. 2013;12(5):814–22.

Publisher's Note